NASA TECHNICAL NOTE

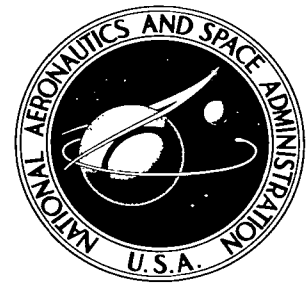

NASA TN D-4019

HEAT-TRANSFER AND TEMPERATURE DISTRIBUTION OF A CONICAL POROUS MEMBRANE DURING PLANETARY ENTRY

by Latif M. Jiji

Ames Research Center
Moffett Field, Calif.

NATIONAL AERONAUTICS AND SPACE ADMINISTRATION • WASHINGTON, D. C. • JUNE 1967

NASA TN D-4019

HEAT-TRANSFER AND TEMPERATURE DISTRIBUTION OF A CONICAL POROUS MEMBRANE DURING PLANETARY ENTRY

By Latif M. Jiji

Ames Research Center
Moffett Field, Calif.

NATIONAL AERONAUTICS AND SPACE ADMINISTRATION

For sale by the Clearinghouse for Federal Scientific and Technical Information
Springfield, Virginia 22151 – CFSTI price $3.00

HEAT-TRANSFER AND TEMPERATURE DISTRIBUTION OF A CONICAL POROUS MEMBRANE DURING PLANETARY ENTRY

By Latif M. Jiji

Ames Research Center

SUMMARY

An approximate analysis is made of the stagnation point heating rate and surface temperature of a conical porous membrane used as a decelerator during planetary entry of vehicles of low ballistic parameter. Ideal gas approximations were used. Order of magnitude variations of the porosity and ballistic parameter, as well as variations in cone angle, were made to find their gross effect on the wall temperature of the membrane. Also, the wall temperature was determined for an order of magnitude variation in the distance rearward along the membrane from the stagnation point. Porosity was found to have an adverse effect on the wall temperature. To avoid high wall temperatures it was necessary to use unrealistic values of ballistic parameter and cone angle.

INTRODUCTION

Decreasing the ballistic parameter, W/C_DA, for a given sized vehicle changes the entry trajectory and decreases the maximum heating rate. A number of variable-drag devices have been considered for possible use during entry into a planetary atmosphere. In particular, deployable and variable-geometry configurations have received considerable attention recently. Examples are the Avco Drag Brake (ref. 1), the "tension structure" (ref. 2), and the Rotornet (refs. 3 and 4). These decelerators may be competitive with the ablation-cooled systems when their basic structural material is lightweight, porous, flexible membranes. Furthermore, varying the frontal area of the decelerator offers a means of modulating drag for controlling the trajectory.

The surface of decelerators is cooled by reradiation so that the equilibrium wall temperatures have to be within the operational level of the membrane material. To establish the potential value of decelerators it is essential to determine the aerodynamic heating and the surface temperature of porous membranes in a hypersonic stream. Theoretical as well as experimental studies of flow configurations and heat-transfer characteristics of such systems are meager. Flow patterns and stagnation point heating of a porous membrane were investigated analytically in reference 5. A study of the heat transfer to a highly porous nose cap was carried out in reference 6.

The purpose of this paper is to investigate the effect of porosity on the heating rate and surface temperature at the stagnation point and on the conical skirt of a porous blunted cone during entry. Based on ideal gas approximations, expressions are derived showing the influence of porosity and cone angle on the aerodynamic heating and wall temperature. Calculations are made to illustrate these effects for typical trajectories of vehicles with low W/C_DA. In this report, a low value of W/C_DA is taken to be 1.0 lb/ft^2, or less.

NOTATION

A	area, ft^2
C_D	drag coefficient
C_n	nozzle flow coefficient
C_{p_m}	specific heat at constant pressure, evaluated at $1/2(T_t + T_w)$, $Btu/lb_m\text{-}^oF$
g	local gravitational acceleration, ft/sec^2
g_c	gravitational constant of proportionality, 32.2 $lb_m\text{-}ft/lb_f\text{-}sec^2$
H	enthalpy, Btu/lb_m
k	ratio of specific heats
M	Mach number
$\dot{m}$	mass flow rate, lb_m/sec
p	pressure, lb_f/ft^2
P	porosity
P_c	critical porosity
Pr	Prandtl number
q	heat-transfer rate, $Btu/sec\text{-}ft^2$
R	radius of curvature, ft
R_g	gas constant, $ft\text{-}lb_f/lb_m\text{-}^oR$
R_o	radius of the earth, ft
T	temperature, ^oR

V_∞ free-stream velocity, ft/sec

V_o entry velocity, ft/sec

V_w suction velocity at wall, ft/sec

VF view factor

W vehicle weight, lb_f

X_c axial distance, measured from the virtual apex of blunted cone, ft

Y altitude, ft

Y_o entry altitude, ft

β pressure gradient parameter ($\beta = 1/2$ for a spherical stagnation point and $\beta = 0$ for a cone)

γ_o entry angle

δ half-cone angle, deg

ϵ surface emissivity

μ viscosity, lb_f-sec/ft^2

ρ mass density, lb_m/ft^3

ρ_o mass density at sea level, lb_m/ft^3

σ Boltzmann's constant, 0.48×10^{-12} Btu/sec-ft^2 $^oR^4$

ψ_c conical skirt suction heat-transfer parameter, equation (16)

ψ_s stagnation point suction heat-transfer parameter, equation (11)

Subscripts

e external to boundary layer

f fiber

imp impermeable

n nose cap

r radiation

s stagnation point

suc	suction (porous surface)
t	stagnation state
w	wall
∞	free stream
*	sonic section

ANALYSIS

The physical system under consideration is a blunted porous conical membrane in hypersonic flow at zero angle of attack (see fig. 1). The flow over a porous surface in hypersonic flight is complex; thus to analyze the aerodynamic heating of such a system, simplified flow patterns are assumed.

Flow Patterns

Flow patterns at the stagnation region of a porous nose cap vary with the porosity. At high porosities discrete detached shocks form over the individual fibers as shown in figure 2(a). As the porosity is decreased, the shocks interact and ultimately coalesce into a single detached shock. The critical porosity, P_c, is defined as the minimum porosity for which there is no spillage (i.e., the entire free-stream flow passes through the porous surface). This flow configuration is shown in figure 2(b). At porosities lower than P_c the flow through the pores is choked and spillage takes place as illustrated in figure 2(c). At some lower limit of porosity, which may be considerably less than P_c, the detached shock must obviously approach that of a solid nose cap. Thus for small porosities it is possible to treat the flow near the surface as boundary-layer flow with surface suction.

One-dimensional, nonviscous, compressible flow relations for an ideal gas are used to obtain an expression for the critical porosity, P_c, at the stagnation point (appendix A):

$$P_c = \frac{\left(\frac{2k}{k+1} M_\infty^2 - \frac{k-1}{k+1}\right)^{\frac{1}{k-1}}}{\left(\frac{\frac{k+1}{2} M_\infty^2}{1 + \frac{k-1}{2} M_\infty^2}\right)^{\frac{k}{k-1}}} \frac{M_\infty}{\left[\left(\frac{2}{k+1}\right)\left(1 + \frac{k-1}{2} M_\infty^2\right)\right]^{\frac{k+1}{2(k-1)}}} \tag{1}$$

Equation (1) is plotted in figure 3 for various values of the ratio of specific heats, k, to indicate the approximate real gas effects. Since k decreases with increasing Mach number (up to M = 25), figure 3 indicates that the critical porosity for hypersonic speeds is approximately 1/3.

The flow pattern over the conical skirt is complex; however, at low porosities (lower than P_c), the flow may again be treated as boundary-layer flow with surface suction. The detached shock over the conical surface for this flow pattern approaches that over the corresponding portion of a blunted solid cone.

Aerodynamic Heating

Analysis of the aerodynamic heating is based on the following two models:

(1) Discrete shocks
(2) Boundary-layer surface suction

In both models the angle of attack is assumed to be zero.

Heat transfer to fibers with discrete shocks.- In this flow pattern each fiber acts as a blunt body in a hypersonic stream. Since the heat-transfer rate is maximum at the stagnation point, attention is to be focused on this region of the fiber. The convective heat-transfer rate at the stagnation point of a sphere of radius R is given by (see refs. 7-9):

$$q_s = \frac{17{,}000}{\sqrt{R}} \left(\frac{\rho_\infty}{\rho_o}\right)^{0.5} \left[\frac{V_\infty}{\sqrt{g(R_o + Y)}}\right]^{3.15} \tag{2}$$

Using this expression limits the analysis to velocities at which the radiative heating can be ignored in comparison to the convective heating.

Equation (2) may be used for comparing the heat-transfer rate at the stagnation point of a cylindrical fiber of radius R_f with that of a solid nose cap of radius R_n. For a cylinder and a sphere of the same radius, equation (2) differs only by a factor of $1/\sqrt{2}$. The resulting expression for the ratio of the fiber to nose cap heat transfer is:

$$\frac{q_f}{q_n} = \left(\frac{R_n}{2R_f}\right)^{1/2} \tag{3}$$

For the range of nose cap to fiber radii considered, the heat-transfer ratio can become very large, as shown in figure 4. It is clear that the heat-transfer rate to the individual fibers is much greater than that at the stagnation point of a nose cap. Therefore, it becomes obvious that porosities larger than the critical value cannot be tolerated.

Heat transfer to porous surface with boundary-layer suction.- For porosities less than the critical porosity, P_c, the flow over a porous surface may be approximated by boundary-layer flow with surface suction. Limited work on this problem has been done for supersonic flow. A theoretical analysis of the effect of mass injection through the boundary layer on heat transfer around blunt bodies of revolution is given in reference 10. In reference 11 the analysis was applied to suction by changing the sign of the mass flow term. This theory was found to agree well with experimental findings (ref. 11). For laminar flow of partially dissociated air, the effect of suction on heat transfer, as verified in reference 11, is given by:

$$\frac{q_{suc}}{q_{imp}} = 1 + 0.58 \left(\frac{\rho_e \mu_e}{\rho_w \mu_w}\right)^{0.04} (Pr)^{-0.18} B \left(\frac{1 + 0.096\sqrt{\beta}}{1.068}\right) \tag{4}$$

where

$$B = \frac{\rho_w V_w}{q_{imp}} (H_t - H_w)$$

or

$$B = \frac{\rho_w V_w}{q_{imp}} C_{p_m} (T_t - T_w) \tag{5}$$

Equation (4) was correlated in reference 11 for values of the suction parameter B up to 4.4. Since for porous surfaces it is not known a priori that $T_w/T_t \ll 1$, the wall temperature has been retained in equation (5). The parameter β takes into consideration the effect of pressure gradient outside the boundary layer. The stagnation temperature T_t is given by

$$T_t = T_\infty \left(1 + \frac{k - 1}{2} M_\infty^2\right) \tag{6}$$

The suction mass flow rate per unit area, $\rho_w V_w$, is obtained by approximating the flow through the pores with one-dimensional, compressible nozzle flow and assuming that the pressure downstream is low enough for conditions to be sonic at the throat. When the continuity equation is applied at the wall (i.e., the inlet section of the nozzle)

$$\dot{m} = \rho_w V_w A_w$$

or

$$\frac{\dot{m}}{A_*} = \rho_w V_w \frac{A_w}{A_*}$$

Noting that the porosity P is defined as

$$P = \frac{A_*}{A_w}$$

the above becomes

$$\rho_w V_w = \left(\frac{\dot{m}}{A_*}\right) P \tag{7}$$

The maximum flow per unit area, $\dot{m}/A_*$, is given by

$$\frac{\dot{m}}{A_*} = C_n \sqrt{\frac{g_c k}{R_g}\left(\frac{2}{k+1}\right)^{\frac{k+1}{k-1}}} \frac{p_{t_w}}{\sqrt{T_t}} \tag{8}$$

Equations (4), (5), (7), and (8) give

$$\frac{q_{suc}}{q_{imp}} = 1 + 0.58\left(\frac{\rho_e \mu_e}{\rho_w \mu_w}\right)^{0.04} (Pr)^{-0.18} C_n P \sqrt{\frac{g_c k}{R_g}\left(\frac{2}{k+1}\right)^{\frac{k+1}{k-1}}} \frac{C_{p_m}(T_t - T_w) p_{t_w}}{q_{imp}\sqrt{T_t}} \left(\frac{1 + 0.096\sqrt{\beta}}{1.068}\right) \tag{9}$$

In equation (9) p_{t_w} is the stagnation pressure on the porous surface. This may be approximated by the stagnation pressure downstream of the detached shock.

Equation (9) is now applied to two regions: (a) the stagnation point and (b) the conical skirt. Expressions for p_{t_w} and q_{imp} must be obtained.

Stagnation point: The detached shock at the stagnation region of the blunted nose cap may be approximated by a normal shock. The stagnation pressure downstream of the shock, p_{t_w}, is given by

$$\frac{p_{t_w}}{p_\infty} = \frac{\left(\frac{k+1}{2} M_\infty^2\right)^{\frac{k}{k-1}}}{\left(\frac{2k}{k+1} M_\infty^2 - \frac{k-1}{k+1}\right)^{\frac{1}{k-1}}} \tag{10}$$

The heat transfer to an impermeable surface at the stagnation point is given by equation (2).

To determine the effect of suction on the stagnation-point heat transfer, the quantity Ψ_s is defined as

$$\psi_s \equiv \frac{1}{C_n P \sqrt{R_n}} \left(\frac{q_{suc}}{q_{imp}} - 1 \right) \tag{11}$$

Equations (2), (9), and (10) give

$$\psi_s = 0.362 \times 10^{-4} \left(\frac{\rho_o}{\rho_\infty} \right)^{0.5} \left[\frac{\sqrt{g(R_o + Y)}}{V_\infty} \right]^{3.15} \sqrt{\frac{g_c k}{R_g} \left(\frac{2}{k+1} \right)^{\frac{k+1}{k-1}}} C_{p_m} (T_t - T_w) \frac{p_\infty}{\sqrt{T_t}} \frac{\left(\frac{k+1}{2} M_\infty^2 \right)^{\frac{k}{k-1}}}{\left(\frac{2k}{k+1} M_\infty^2 - \frac{k-1}{k+1} \right)^{\frac{1}{k-1}}} \tag{12}$$

In equation (12) the Prandtl number for air is taken as equal to 0.71 and β at the stagnation point is 0.50. The dimensionless ratio $(\rho_e \mu_e / \rho_w \mu_w)^{0.04}$ is assumed to be unity. This is justified since $(\rho_e \mu_e / \rho_w \mu_w)$ is of the order of magnitude of one.

Equation (12) gives the value of ψ_s as a function of altitude for a vehicle of known trajectory.

Conical skirt: Since streamlines are approximately parallel to the conical surface, equation (8) overestimates the suction mass flow rate if the actual stagnation pressure, p_{t_w}, is used. A more realistic estimate can be obtained by replacing p_{t_w} in equations (8) and (9) by the static pressure at the wall, p_w. If the effect of blunting is neglected, then from Newtonian flow approximations the static pressure over the conical skirt is given by

$$\frac{p_w}{p_\infty} = 1 + k M_\infty^2 \sin^2 \delta \tag{13}$$

For cones in dissociated air the shock may remain attached for half angles up to 60°. The Newtonian approximation underestimates the actual value of p_w by approximately 6 percent for values of δ ranging from 0° to 60° (ref. 12).

The heat-transfer rate to an impermeable cone is correlated with the free-stream velocity, density, and cone angle in reference 13. The following correlation equation applies to laminar flow over pointed cones at zero angle of attack:

$$q_{imp} = \frac{535}{\sqrt{X_c}} \left(\frac{\rho_\infty}{\rho_o} \right)^{0.5} \left(\frac{V_\infty}{10^4} \right)^{3.35} \sin 2\delta \tag{14}$$

Since blunting has a minor effect on the heat-transfer characteristics when the distance X_c is measured from the virtual apex of the blunted cone (ref. 7), equation (14) can be applied to blunted cones.

When equations (13) and (14) are substituted into equation (9), and since $\beta = 0$ for a cone, the following is obtained:

$$\psi_c = 1.08\times10^{-3}\left(\frac{\rho_\infty}{\rho_o}\right)^{0.5}\left(\frac{10^4}{V_\infty}\right)^{3.35}\sqrt{\frac{g_c k}{R_g}\left(\frac{2}{k+1}\right)^{\frac{k+1}{k-1}}}\frac{C_{p_m}(T_t - T_w)}{\sqrt{T_t}}\frac{(1 + kM_\infty^2 \sin^2\delta)p_\infty}{\sin 2\delta} \tag{15}$$

where

$$\psi_c \equiv \frac{1}{C_n P\sqrt{X_c}}\left(\frac{q_{suc}}{q_{imp}} - 1\right) \tag{16}$$

Equilibrium Wall Temperature

To determine the equilibrium wall temperature, the convective heat rate is equated to the heat loss by radiation. Radiation heat-transfer rate is given by

$$q_r = \epsilon(VF)\sigma T_w^4 \tag{17}$$

When equation (2) is written for flow over a cylinder and is combined with equation (17), for discrete shocks,

$$T_w = \left\{\frac{1}{\epsilon(VF)\sigma}\frac{17{,}000}{\sqrt{2R_f}}\left(\frac{\rho_\infty}{\rho_o}\right)^{0.5}\left[\frac{V_\infty}{\sqrt{g(R_o + Y)}}\right]^{3.15}\right\}^{1/4} \tag{18}$$

For flow with boundary layer suction the wall temperature at the stagnation point of a porous nose cap is given by

$$\frac{17{,}000}{\sqrt{R_n}}\left(\frac{\rho_\infty}{\rho_o}\right)^{0.5}\left[\frac{V_\infty}{\sqrt{g(R_o + Y)}}\right]^{3.15} + 0.615\, C_n P\sqrt{\frac{g_c k}{R_g}\left(\frac{2}{k+1}\right)^{\frac{k+1}{k-1}}}\frac{C_{p_m}(T_t - T_w)p_\infty\left(\frac{k+1}{2}M_\infty^2\right)^{\frac{k}{k-1}}}{\sqrt{T_t}\left(\frac{2k}{k+1}M_\infty^2 - \frac{k-1}{k+1}\right)^{\frac{1}{k-1}}} = \epsilon(VF)\sigma T_w^4 \tag{19}$$

Equation (19) is obtained from equations (2), (11), (12), and (17). Similarly, for the conical skirt, equations (14), (15), (16), and (17) give:

$$\frac{535}{\sqrt{X_c}}\left(\frac{\rho_\infty}{\rho_o}\right)^{0.5}\left(\frac{V_\infty}{10^4}\right)^{3.35}\sin 2\delta + 0.576\, C_n P\sqrt{\frac{g_c k}{R_g}\left(\frac{2}{k+1}\right)^{\frac{k+1}{k-1}}\frac{C_{p_m}(T_t - T_w)\rho_\infty}{\sqrt{T_t}}}\left(1 + kM_\infty^2 \sin^2\delta\right) = \epsilon(VF)\sigma T_w^4 \tag{20}$$

APPLICATIONS

To investigate the effect of porosity on the heat-transfer rate and surface temperature distribution, the analysis is applied to vehicles with low ballistic parameters. Three trajectories based on the 1959 ARDC atmosphere (ref. 14) were computed for values of W/C_DA of 0.01, 0.1, and 1.0 lb_f/ft^2. Figure 5 shows these trajectories for an equatorial entry at 25,000 ft/sec, 500,000-ft initial altitude, and with an initial entry angle of -5°.

The suction heat-transfer parameter ψ_s at the stagnation point of a porous nose cap determined from equation (12) is plotted in figure 6 for a wall temperature of 1000° R. For the conical skirt, equation (16) is plotted in figure 7 for half-cone angles of 15°, 45°, and 60°. Note that the ballistic parameter W/C_DA has an appreciable effect on both ψ_s and ψ_c.

Stagnation wall temperature profiles for fibers with individual shocks are plotted in figure 8 (eq. (18)) for fiber radii of 0.0025, 0.0125, and 0.025 inch. Even for a ballistic parameter as low as 0.01 lb_f/ft^2 the resulting temperatures are excessively high. Thus configurations which result in discrete shocks over the individual fibers cannot be tolerated.

For a porous nose cap with a boundary-layer-suction flow pattern, temperature profiles at the stagnation region of a 2-foot radius nose cap are plotted in figure 9. Profiles are shown for values of C_nP ranging from 0 to 0.60; $C_nP = 0$ corresponds to a solid surface, while $C_nP = 0.60$ is an approximate upper limit corresponding to the critical porosity for $k = 1.4$. For values of $C_nP = 0.01$, the effect of suction on the temperature distribution is negligible. However, for $C_nP = 0.1$ the effect is significant, particularly for a ballistic parameter of 1.0 lb_f/ft^2 or greater. It is therefore desirable to have as inefficient a nozzle as possible, even for low values of porosity.

Figure 10 gives the effect of ballistic parameter on the maximum stagnation-point wall temperature for various values of C_nP. The wall temperature is observed to increase rapidly with W/C_DA. For reasonable values of W/C_DA for this concept, about 1.0 lb_f/ft^2, C_nP of 0.1 increases the maximum wall temperature relative to the nonporous value over 50 percent. On the other hand, for $W/C_DA = 0.01$ lb_f/ft^2 the corresponding increase in the maximum temperature is about 10 percent.

Temperature profiles at the conical skirt for X_c = 10 feet are shown in figure 11 for various values of C_nP, W/C_DA, and δ. At $\delta = 60^\circ$ (fig. 11(c)) the porosity effect is significant for C_nP as low as 0.10 for $W/C_DA = 1.0$ lb_f/ft^2. These profiles indicate that the adverse effect of porosity on the temperature becomes more severe as W/C_DA and/or δ are increased.

Figure 12 shows the variation of maximum wall temperature with X_c. It is observed that the effect of changing X_c on the wall temperature is less pronounced when the effect of suction is appreciable (i.e., at high values of W/C_DA and/or δ).

Temperature distribution charts for both the nose cap and the conical skirt indicate that if W/C_DA could be reduced to 0.01 lb_f/ft^2, the maximum wall temperature could be maintained at reasonable low levels. However, in this case the ratio of payload to weight for this type of retardation loses its advantage over that of the ablative heat shield with parachute recovery system.

A major factor in the design of a rotating conical skirt is the size required. For example, to recover a payload of 500 lb (including decelerator weight) with $C_D = 1$ would require a skirt 25 feet in diameter for $W/C_DA = 1.0$ lb_f/ft^2. If, to avoid the severe heating problem, W/C_DA were reduced to 0.01 lb_f/ft^2, the diameter would increase to 250 feet. These calculations were made for a value of k of 1.4. While real gas effects can be evaluated only from real gas properties, rather than ideal gas relations, limited calculations were made for $k = 1.1$ in an attempt to estimate real gas effects. Wall temperatures were found to be approximately 15 percent lower for $k = 1.1$ than for 1.4.

CONCLUDING REMARKS

The wall temperature for a porous conical membrane during planetary entry is excessively high when discrete shocks form over the individual fibers; thus membrane porosities must be less than the critical porosity. For the boundary layer suction flow pattern, associated with low porosities, and reasonable values of W/C_DA (about 1.0 lb_f/ft^2) the temperature increase due to porosity is too severe even for relatively low porosity. For lower values of W/C_DA, the payload-to-weight ratio loses its advantage over that of the ablative heat shield with parachute recovery.

Ames Research Center
National Aeronautics and Space Administration
Moffett Field, Calif., 94035, Feb. 7, 1967
124-07-02-27-00-21

APPENDIX A

CRITICAL POROSITY

For one-dimensional isentropic flow of a perfect gas, the mass flow per unit area is given by:

$$\frac{\dot{m}}{A} = \sqrt{\frac{kg_c}{R_g}} \frac{p_t}{\sqrt{T_t}} \frac{M}{\left(1 + \frac{k-1}{2} M^2\right)^{\frac{k+1}{2(k-1)}}} \tag{A1}$$

If equation (A1) is applied to the flow upstream of the shock,

$$\frac{\dot{m}}{A_w} = \sqrt{\frac{kg_c}{R_g}} \frac{p_{t_\infty}}{\sqrt{T_{t_\infty}}} \frac{M_\infty}{\left(1 + \frac{k-1}{2} M_\infty^2\right)^{\frac{k+1}{2(k-1)}}} \tag{A2}$$

If it is assumed that the pressure downstream of the porous surface is low enough to give sonic speed at the throat, equation (A1) gives

$$\frac{\dot{m}}{A_*} = \sqrt{\frac{kg_c}{R_g}\left(\frac{2}{k+1}\right)^{\frac{k+1}{k-1}}} \frac{p_{*_t}}{\sqrt{T_{*_t}}} \tag{A3}$$

Equations (A2) and (A3) give the critical porosity

$$P_c = \frac{A_*}{A_w} = \frac{p_{t_\infty}}{p_{*_t}} \sqrt{\frac{T_{*_t}}{T_{t_\infty}}} \frac{\left(\frac{k+1}{2}\right)^{\frac{k+1}{2(k-1)}}}{\left(1 + \frac{k-1}{2} M_\infty^2\right)^{\frac{k+1}{k-1}}} M_\infty \tag{A4}$$

The stagnation temperature ratio T_{*_t}/T_{t_∞} is equal to unity. The stagnation pressure ratio is obtained from normal shock relations

$$\frac{p_{*_t}}{p_{t_\infty}} = \frac{\left(\dfrac{\frac{k+1}{2} M_\infty^2}{1 + \frac{k-1}{2} M_\infty^2}\right)^{\frac{k}{k-1}}}{\left(\frac{2k}{k+1} M_\infty^2 - \frac{k-1}{k+1}\right)^{\frac{1}{k-1}}} \tag{A5}$$

Equations (A4) and (A5) give

$$P_c = \frac{\left(\frac{2k}{k+1} M_\infty^2 - \frac{k-1}{k+1}\right)^{\frac{1}{k-1}}}{\left(\dfrac{\frac{k+1}{2} M_\infty^2}{1 + \frac{k-1}{2} M_\infty^2}\right)^{\frac{k}{k-1}}} \frac{M_\infty}{\left[\frac{2}{k+1}\left(1 + \frac{k-1}{2} M_\infty^2\right)\right]^{\frac{k+1}{2(k-1)}}} \tag{A6}$$

REFERENCES

1. Anon.: Study of a Drag Brake Satellite Recovery System. Aeronautical Systems Division, ASD-TR-61-348, Jan. 1962.

2. Anderson, M. S.; Robinson, J. C.; Bush, H. G.; and Fralich, R. W.: A Tension Shell Structure for Application to Entry Vehicles. NASA TN D-2675, 1965.

3. Schuerch, H. U.; and MacNeal, R.: Deployable Centrifugally Stabilized Structures for Atmospheric Entry From Space. NASA CR-69, 1964.

4. Kyser, A. C.: The Rotornet: A High-Performance Hypersonic Decelerator for Planetary Entry. NASA CR-247, 1965.

5. Coplan, M. J.; and Freestone, W. D., Jr.: High Speed Flow and Aerodynamic Heating Behavior of Porous Fibrous Structures. WADD TN 61-58, Oct. 1961.

6. Lorsch, H. G.: Heat Transfer to Porous Nose Caps and Leading Edges of Hypersonic Vehicles and Reentry Aids. Vol. 11 of Advances in Astronautical Sciences, Am. Astronom. Soc., 1963, pp. 752-766.

7. Lees, Lester: Laminar Heat Transfer Over Blunt-Nosed Bodies at Hypersonic Flight Speeds. Jet Propulsion, vol. 26, no. 4, Apr. 1956, pp. 259-269, 274.

8. Chapman, Dean R.: An Approximate Analytical Method for Studying Entry Into Planetary Atmospheres. NASA TR R-11, 1959.

9. Detra, R. W.; Kemp, N. H.; and Riddell, F. R.: Addendum to Heat Transfer to Satellite Vehicles Re-entering the Atmosphere. Jet Propulsion, vol. 27, no. 12, Dec. 1957, pp. 1256-1257.

10. Hidalgo, H.: A Theory of Ablation of Glassy Materials for Laminar and Turbulent Heating. AVCO Res. Rept. 62, June 1959.

11. AVCO-Everett Research Laboratory: A Study of a Drag Brake Satellite Recovery System. Results of Phase I (Dyna-Soar). WADD TR 60-775, Jan. 1961.

12. Feldman, S.: Hypersonic Conical Shocks for Dissociated Air in Thermodynamic Equilibrium. AVCO Res. Rept. 12, May 1957.

13. Schapker, Richard L.: Correlation of Laminar Heating to Cones in High-Speed Flight at Zero Angle of Attack. AIAA J., vol. 1, no. 8, Aug. 1963, pp. 1953-1954.

14. Minzner, R. A.; Champion, K. S. W.; and Pond H. L.: The ARDC Model Atmosphere, 1959. Air Force Surveys in Geophysics No. 115 (AFCRC-TR-59-267) Air Force Cambridge Res. Center, Aug. 1959.

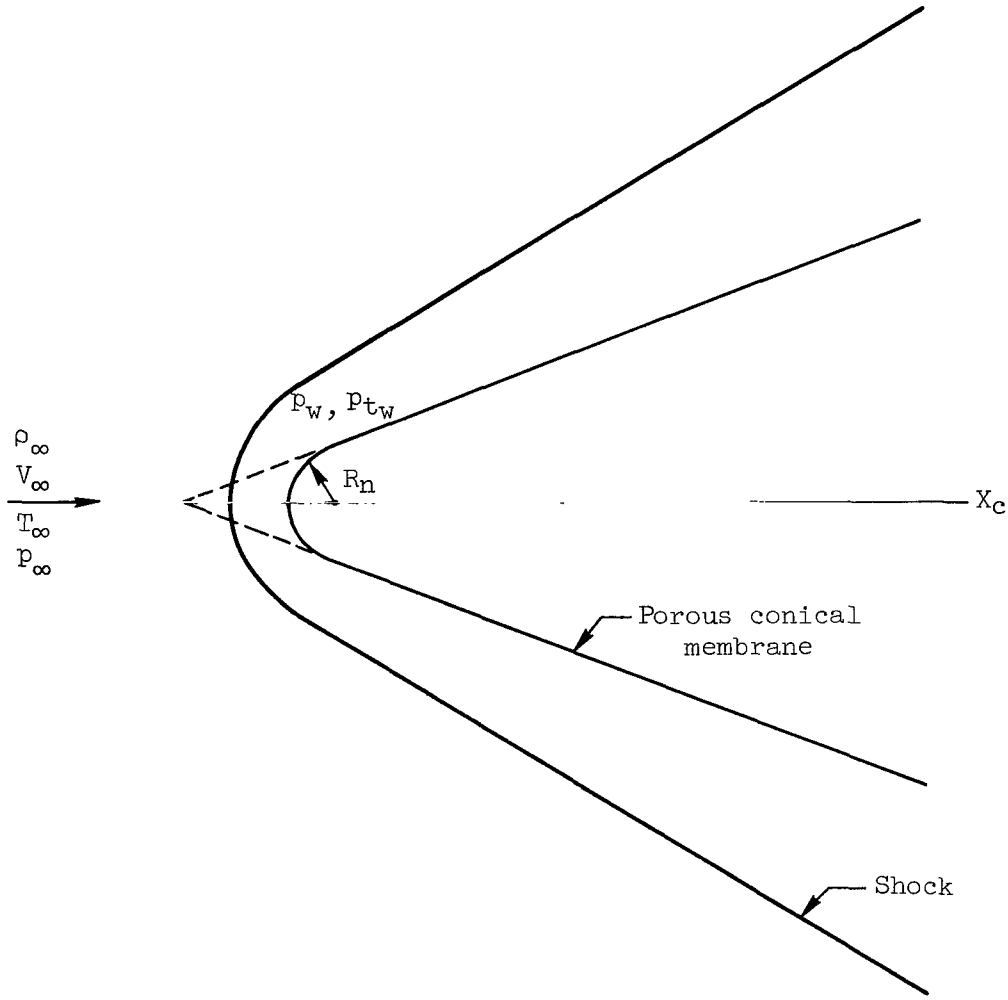

Figure 1.- Conical membrane in hypersonic flight.

(a) $P > P_c$

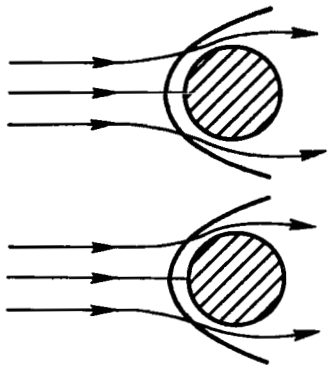

(b) $P = P_c$

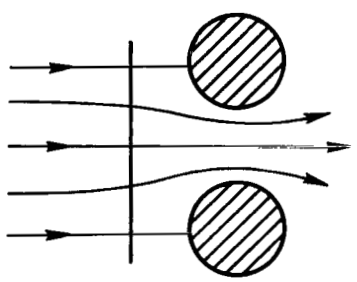

(c) $P < P_c$

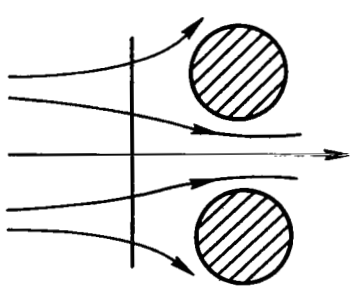

Figure 2.- Flow configurations at the stagnation region of a porous surface in hypersonic flight.

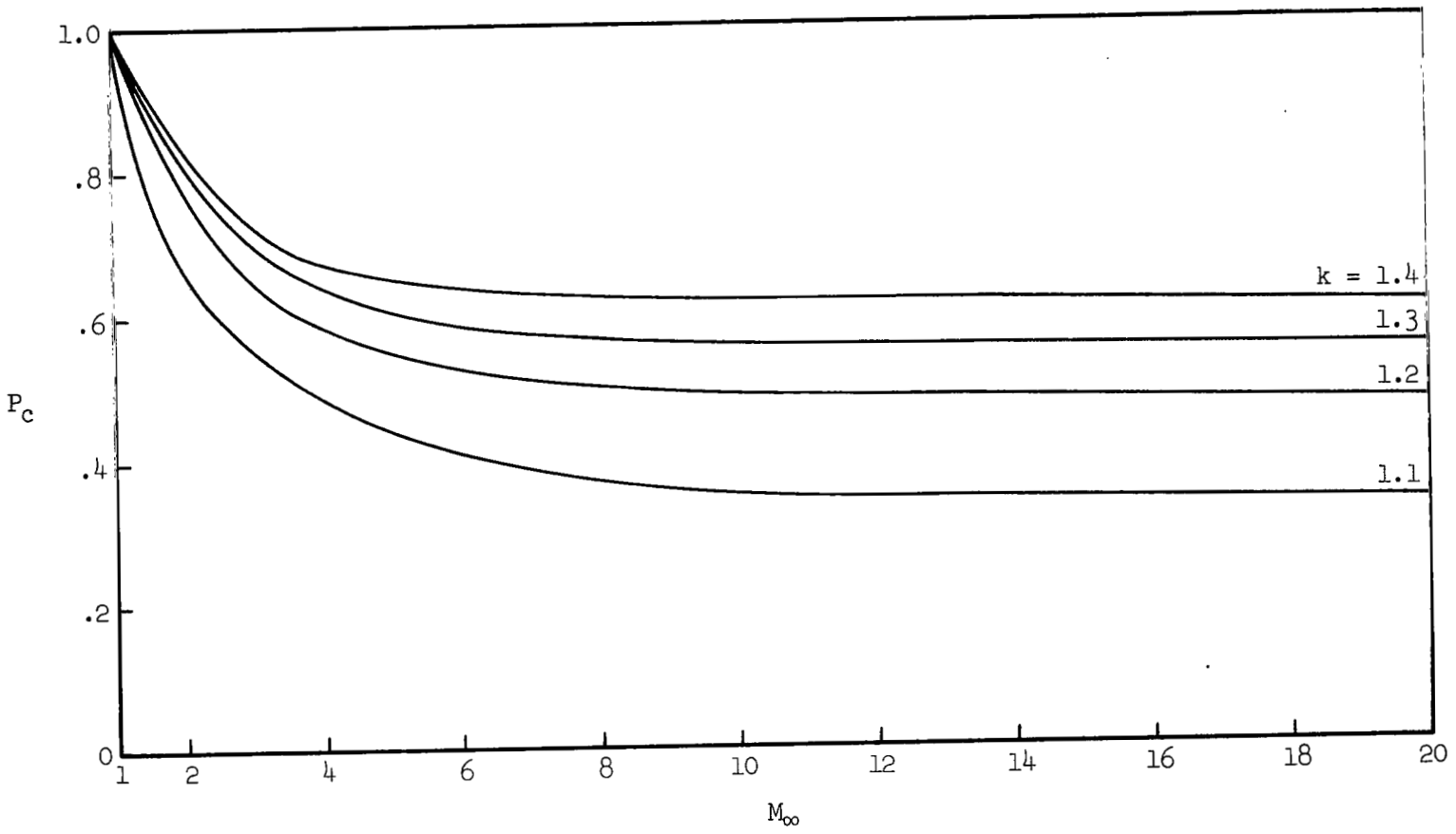

Figure 3.- Effect of flight Mach number and ratio of specific heats on critical porosity.

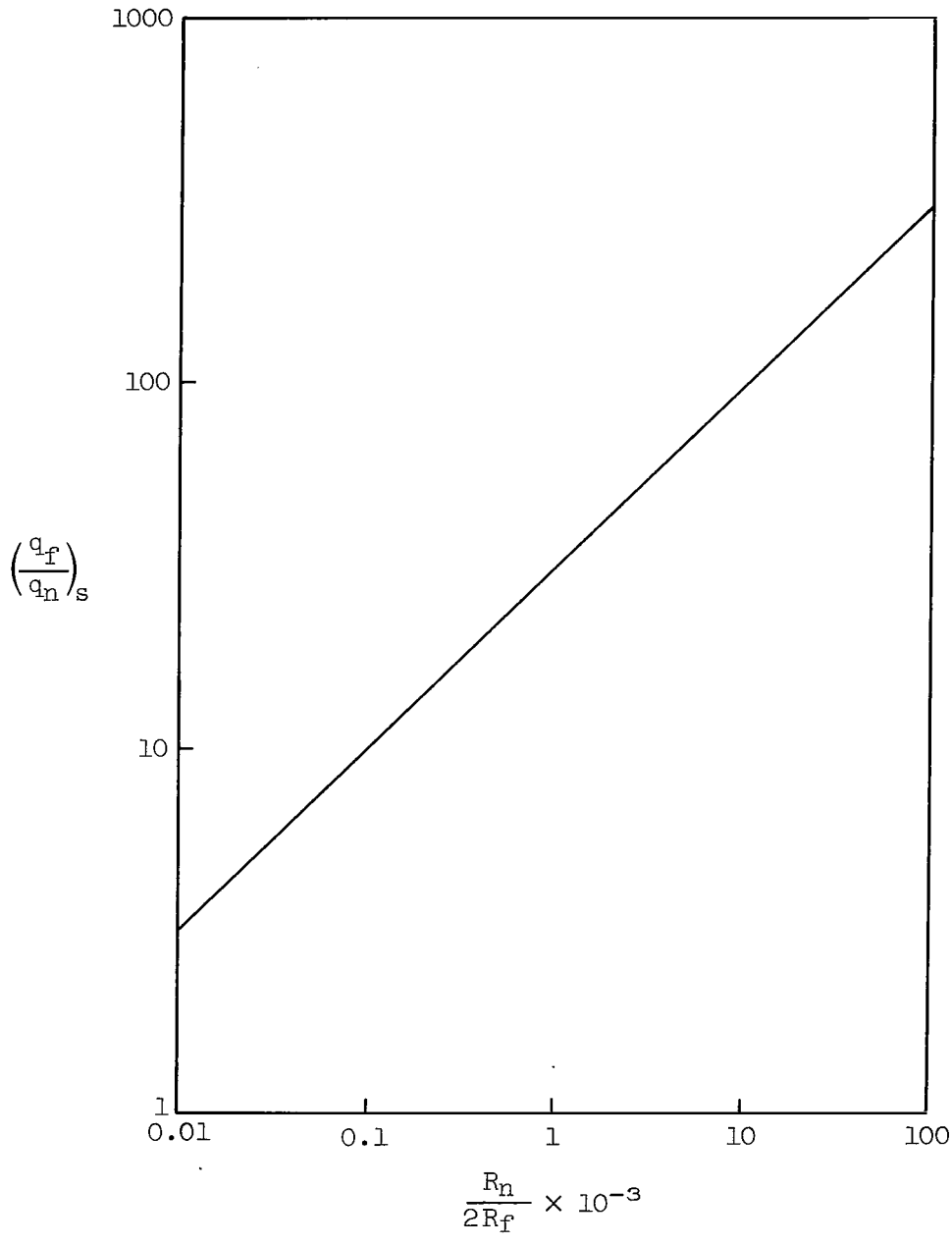

Figure 4.- Heat-transfer ratio at stagnation point of fiber nose cap.

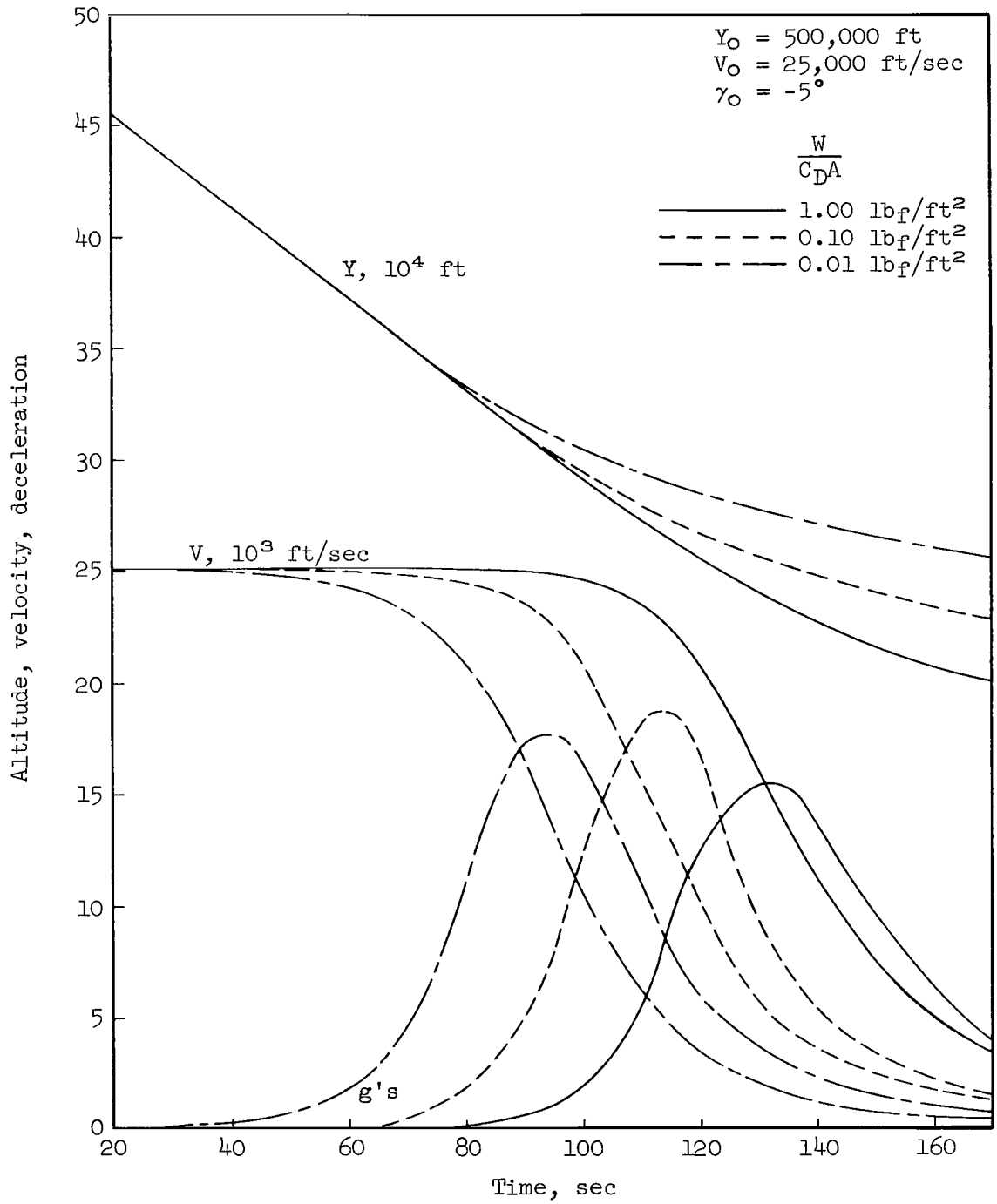

Figure 5.- Vehicle trajectories for earth entry.

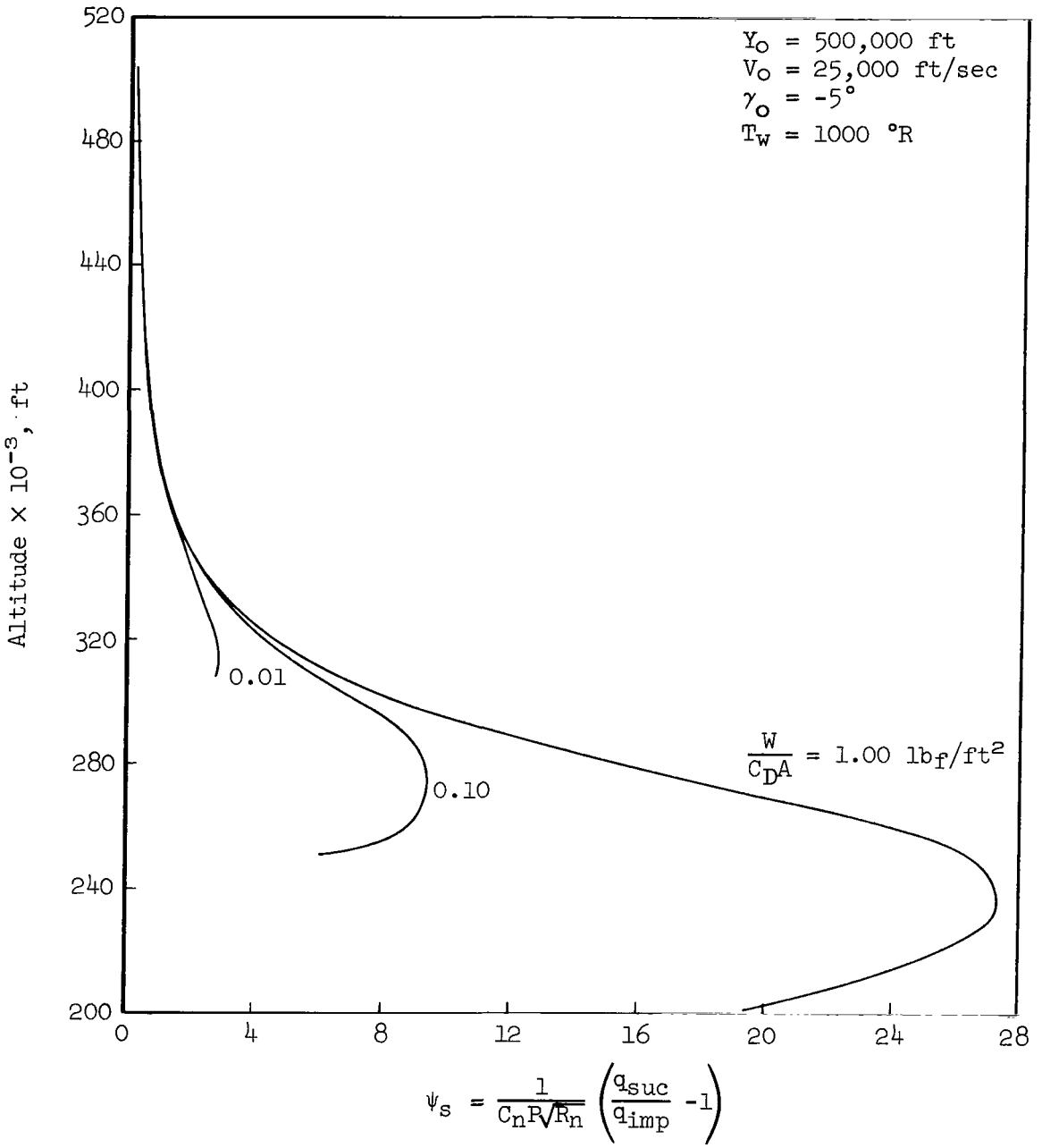

Figure 6.- Heat-transfer parameter at stagnation point with suction.

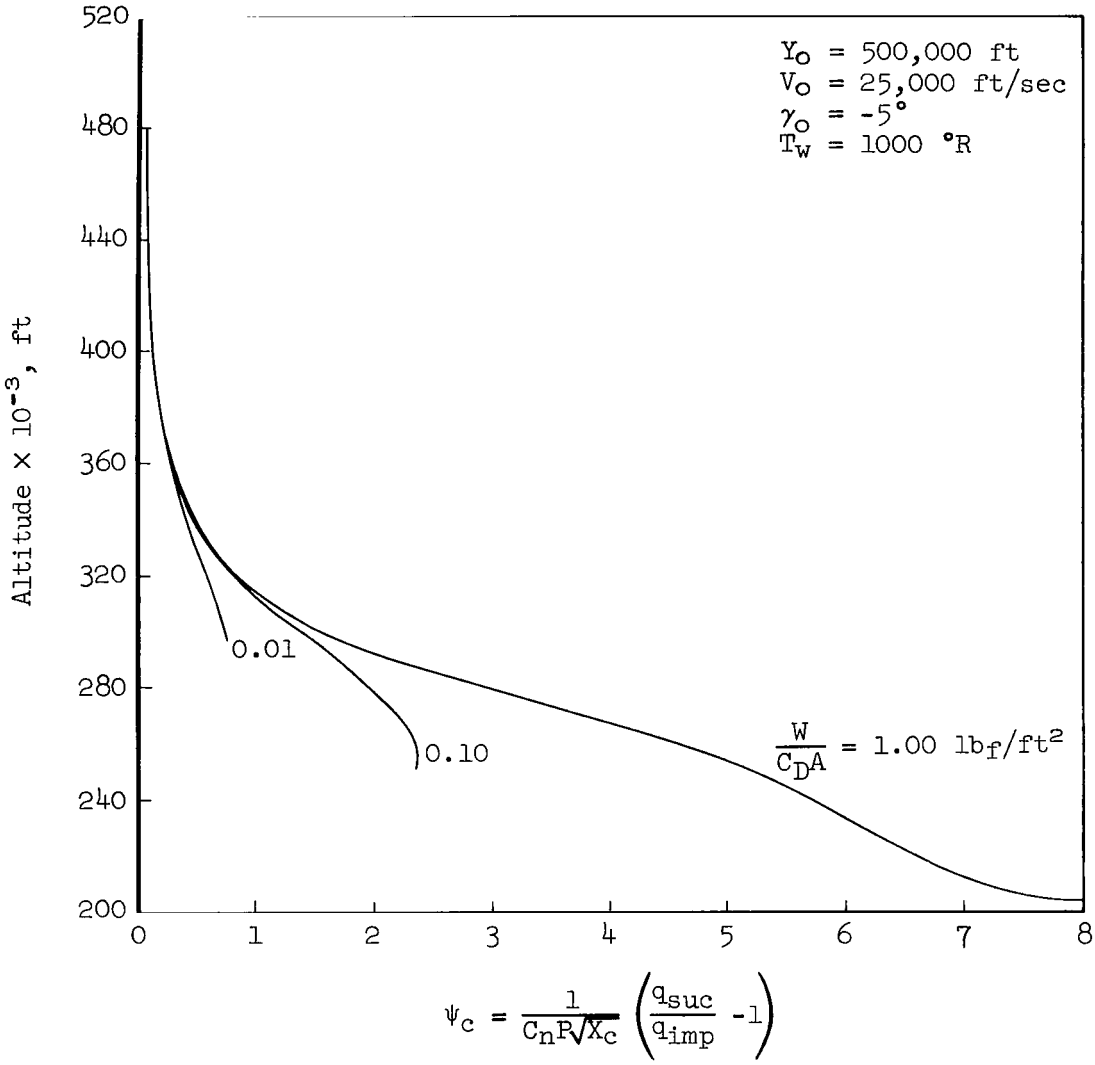

(a) $\delta = 15°$

Figure 7.- Heat-transfer parameter for conical skirt with suction.

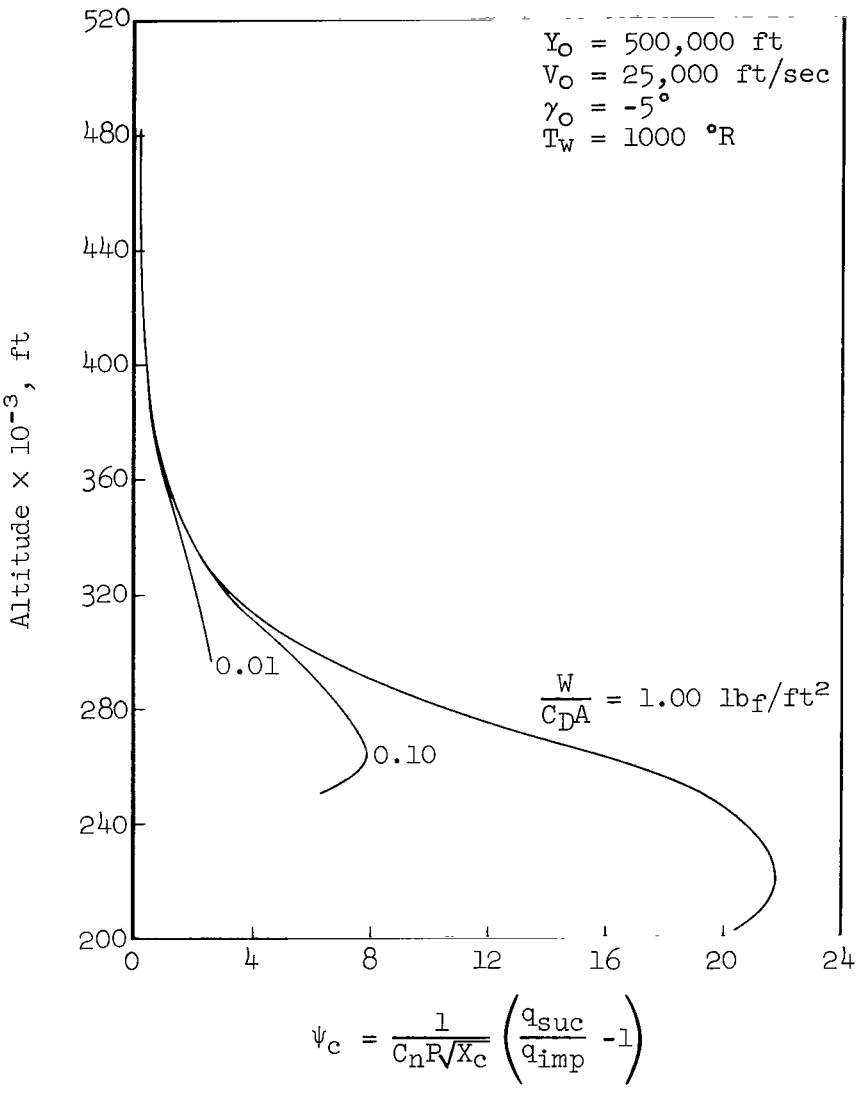

(b) $\delta = 45°$

Figure 7.- Continued.

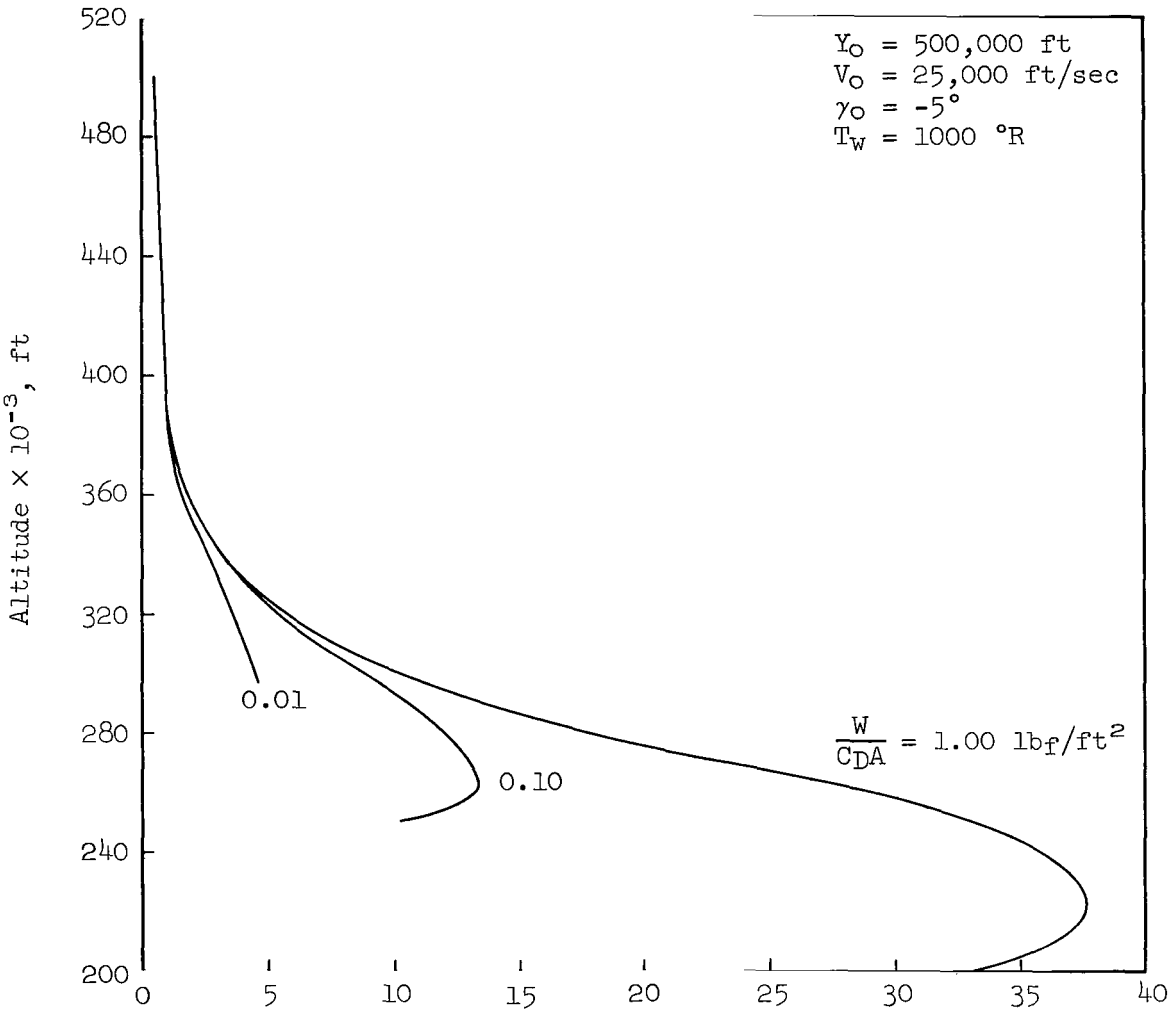

$$\Psi_c = \frac{1}{C_{n_P}\sqrt{X_c}}\left(\frac{q_{suc}}{q_{imp}} - 1\right)$$

(c) δ = 60°

Figure 7.- Concluded.

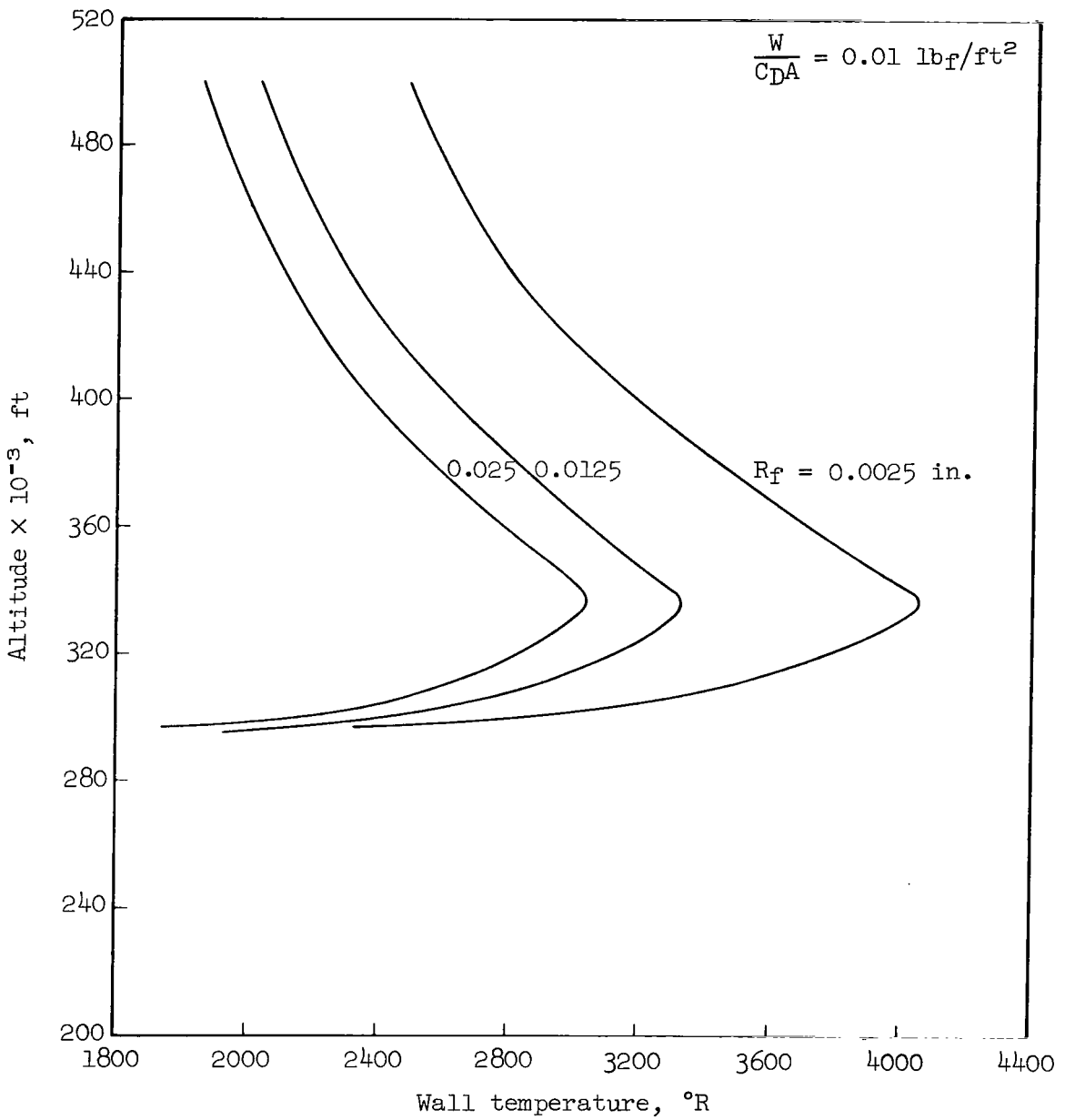

Figure 8.- Wall temperature profiles for fibers with individual shocks; ϵ (VF) = 1.5.

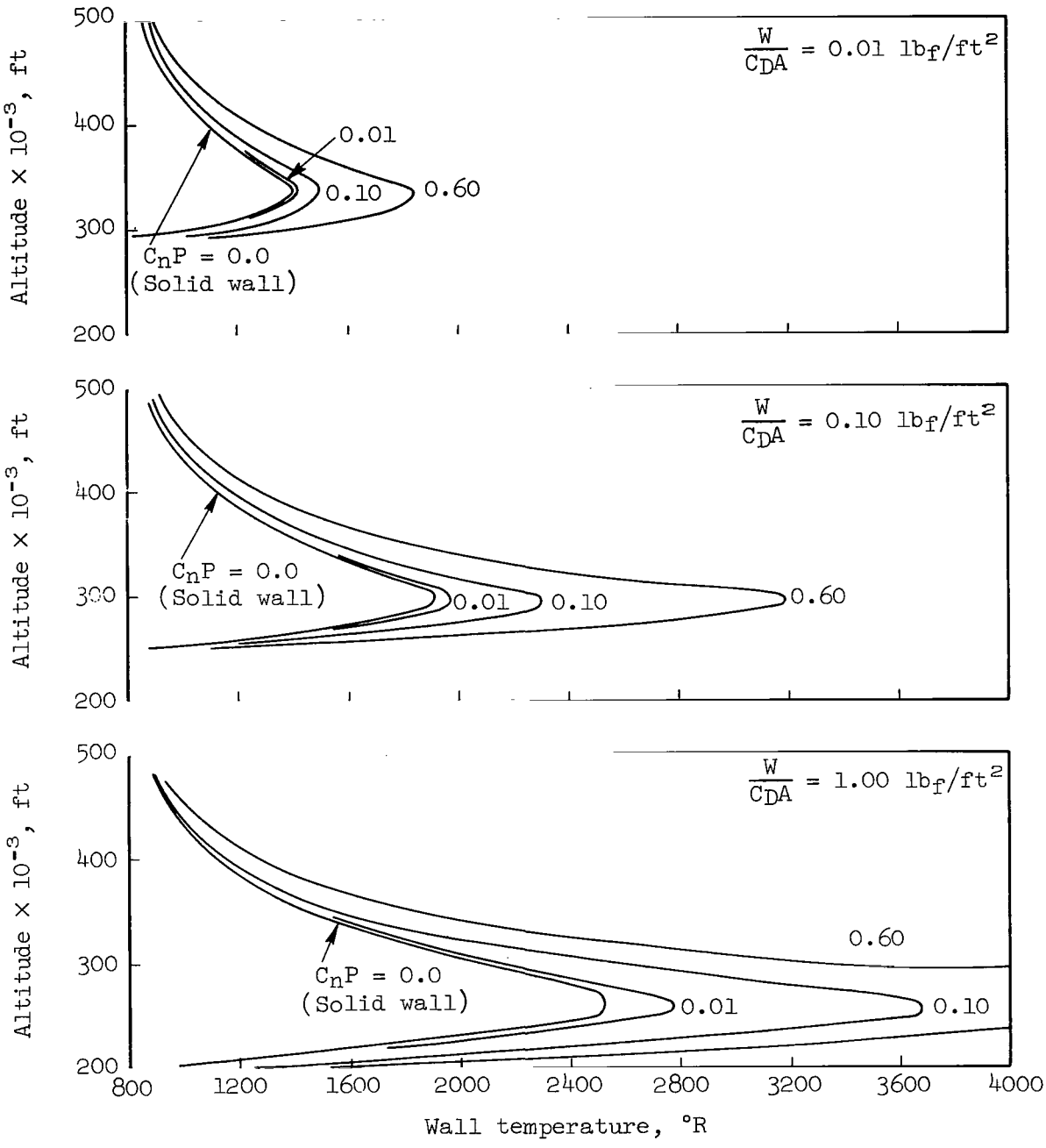

Figure 9.- Wall temperature profiles at the stagnation point of a porous nose cap; ϵ (VF) = 1.5, R_n = 2 feet.

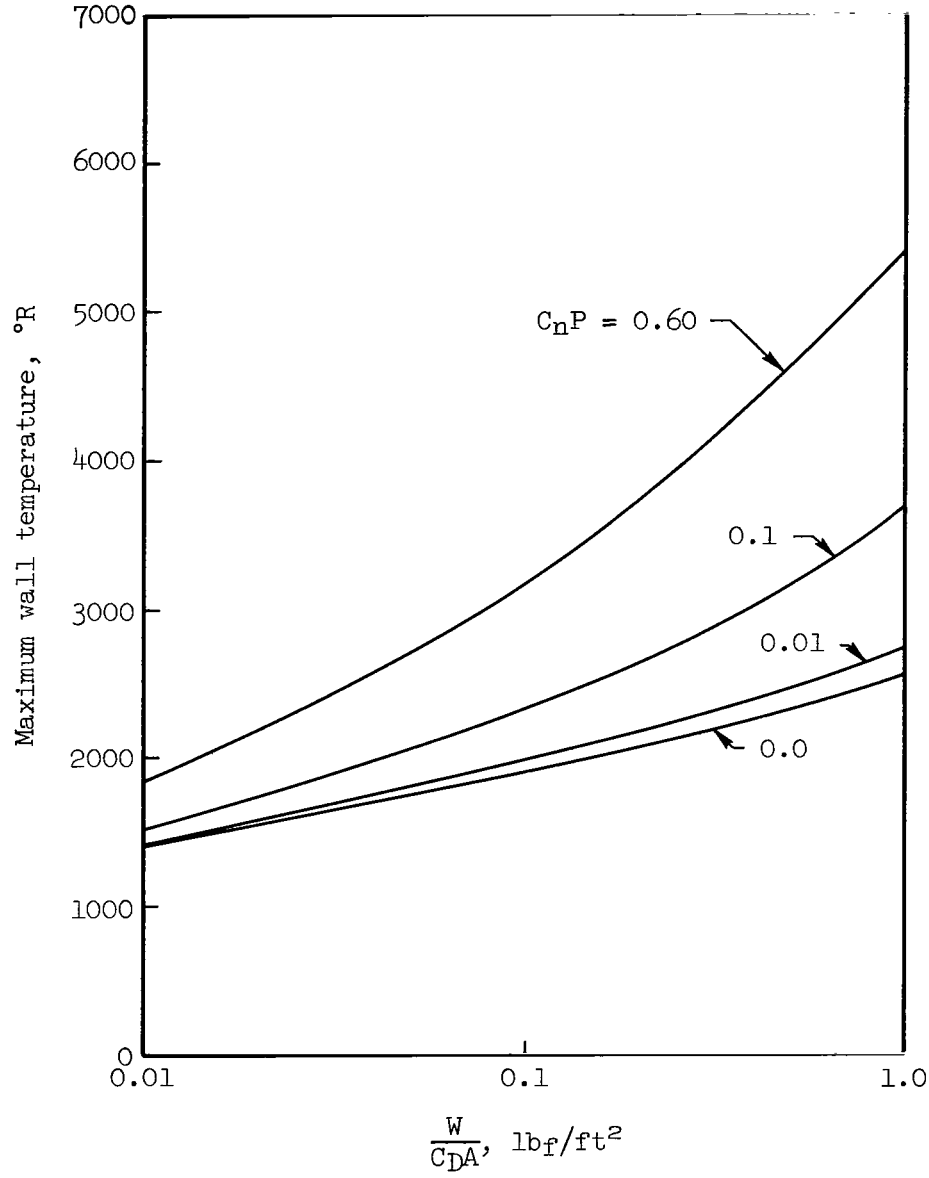

Figure 10.- Maximum stagnation point wall temperature; ϵ (VF) = 1.5, R_n = 2 feet.

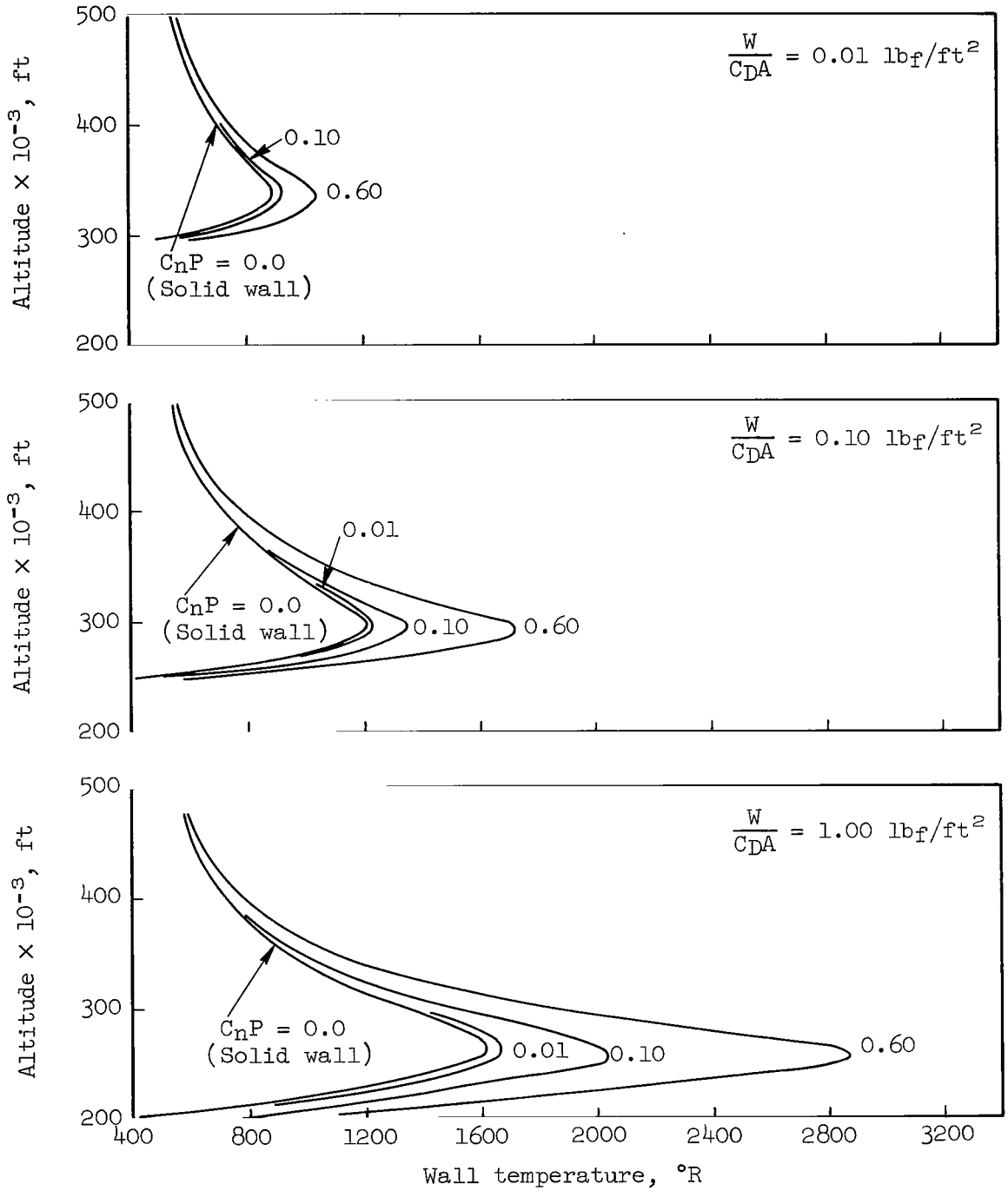

(a) $\delta = 15°$

Figure 11.- Wall temperature profiles for conical skirt; ϵ (VF) = 1.5, X_c = 10 feet.

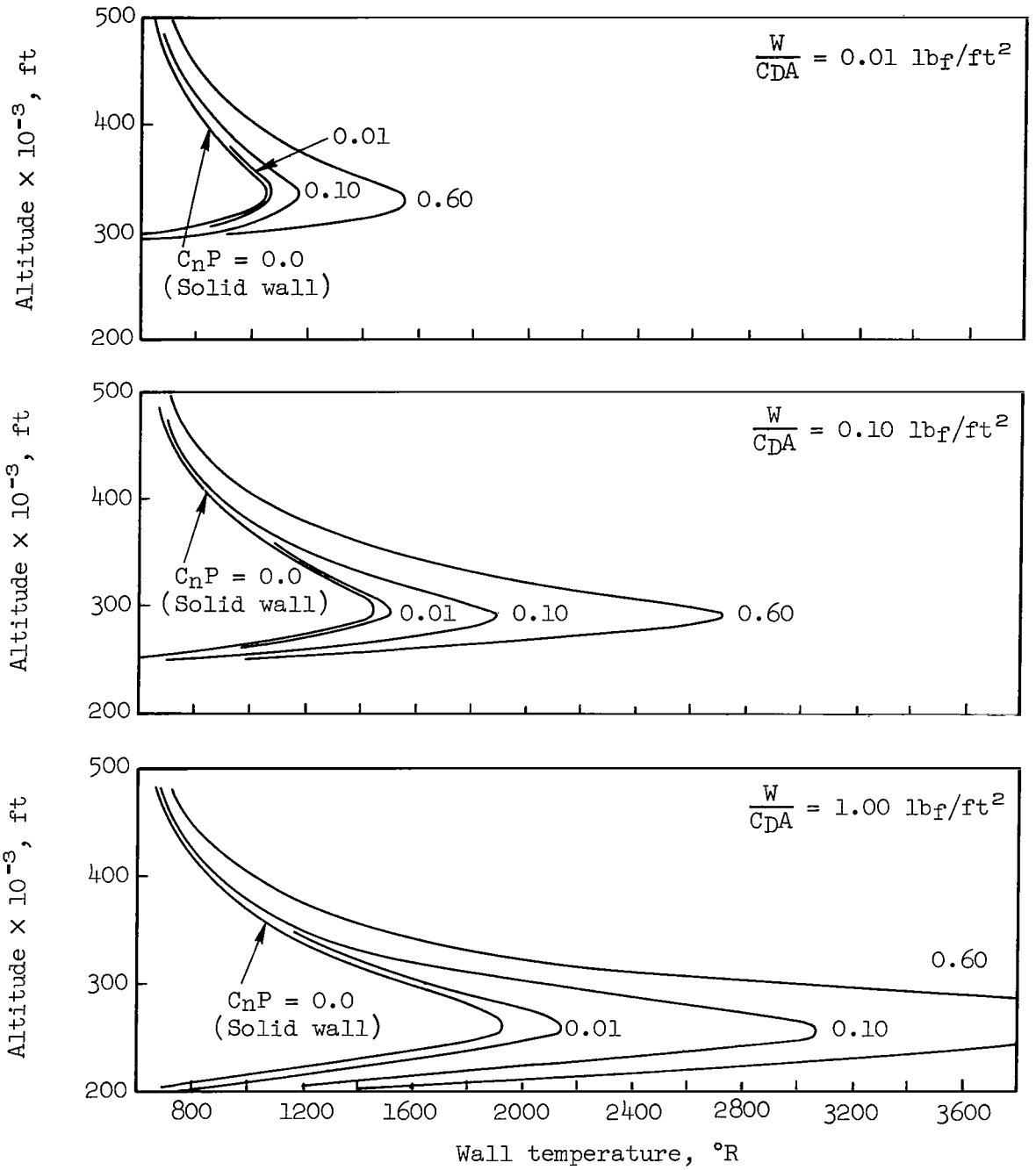

(b) $\delta = 45°$

Figure 11.- Continued.

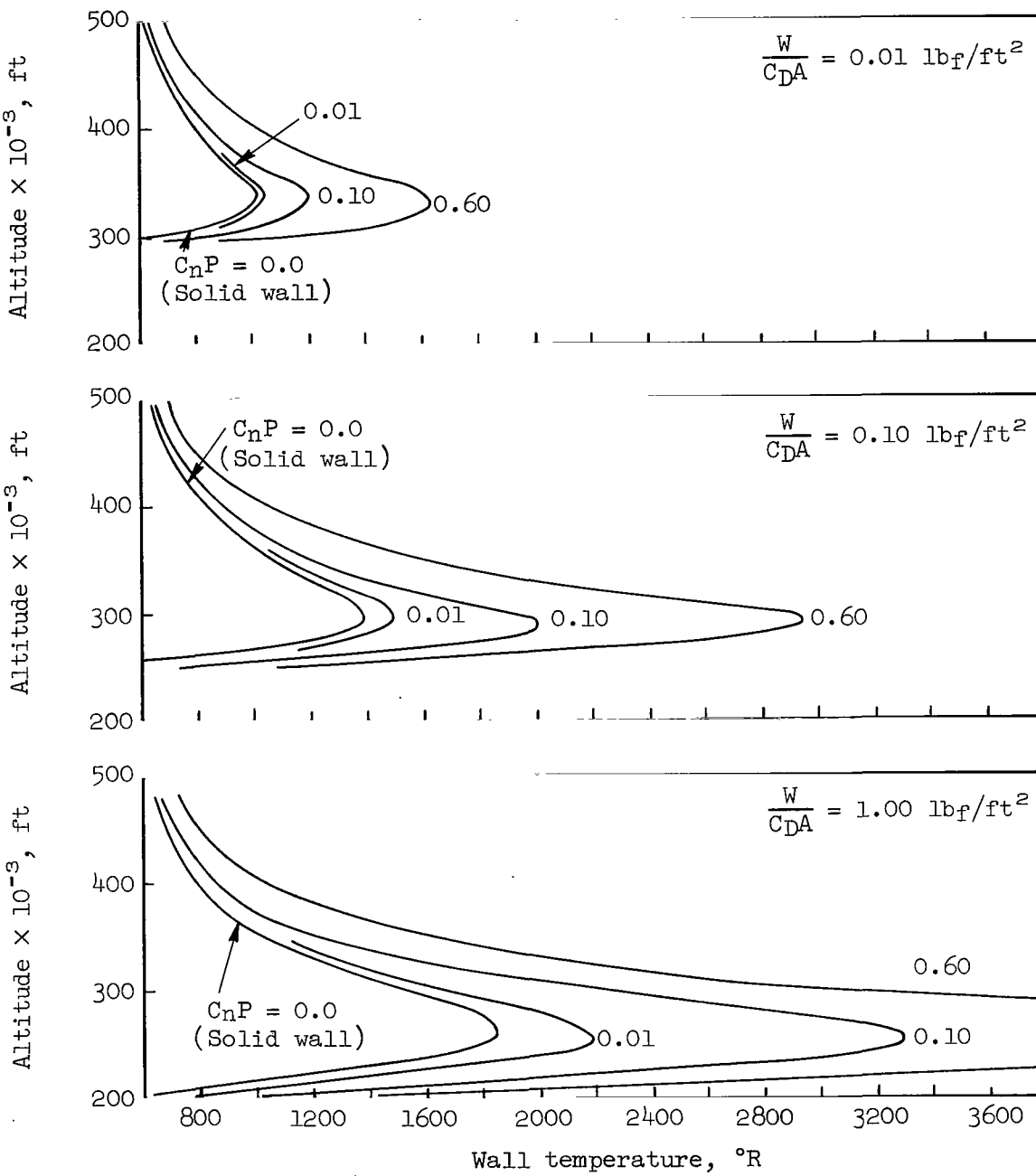

(c) $\delta = 60°$

Figure 11.- Concluded.

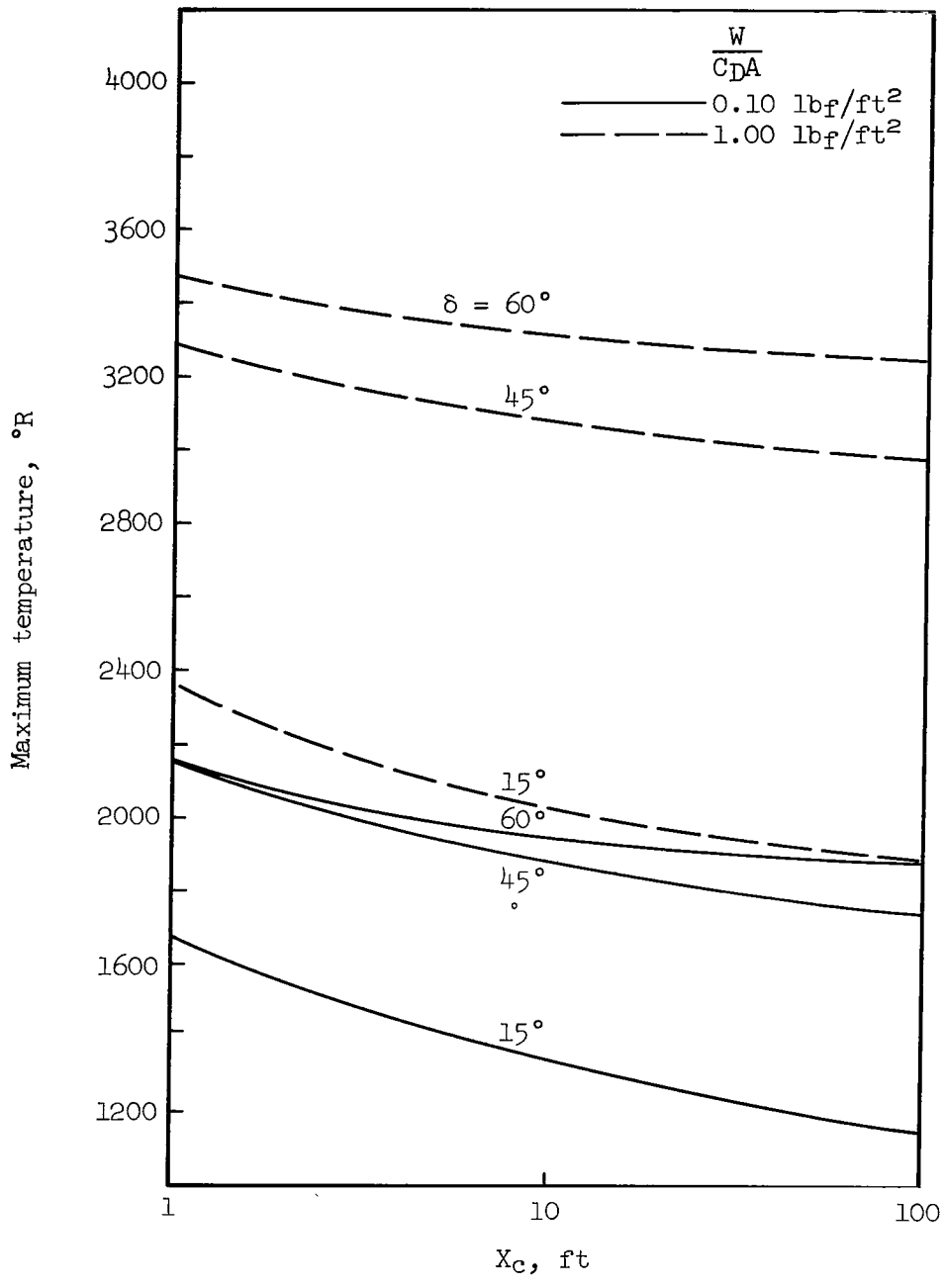

Figure 12.- Effect of X_c on the maximum wall temperature; ϵ (VF) = 1.5, C_nP = 0.1.

NASA-Langley, 1967 —— 33 A-2332

"The aeronautical and space activities of the United States shall be conducted so as to contribute . . . to the expansion of human knowledge of phenomena in the atmosphere and space. The Administration shall provide for the widest practicable and appropriate dissemination of information concerning its activities and the results thereof."

—NATIONAL AERONAUTICS AND SPACE ACT OF 1958

NASA SCIENTIFIC AND TECHNICAL PUBLICATIONS

TECHNICAL REPORTS: Scientific and technical information considered important, complete, and a lasting contribution to existing knowledge.

TECHNICAL NOTES: Information less broad in scope but nevertheless of importance as a contribution to existing knowledge.

TECHNICAL MEMORANDUMS: Information receiving limited distribution because of preliminary data, security classification, or other reasons.

CONTRACTOR REPORTS: Scientific and technical information generated under a NASA contract or grant and considered an important contribution to existing knowledge.

TECHNICAL TRANSLATIONS: Information published in a foreign language considered to merit NASA distribution in English.

SPECIAL PUBLICATIONS: Information derived from or of value to NASA activities. Publications include conference proceedings, monographs, data compilations, handbooks, sourcebooks, and special bibliographies.

TECHNOLOGY UTILIZATION PUBLICATIONS: Information on technology used by NASA that may be of particular interest in commercial and other non-aerospace applications. Publications include Tech Briefs, Technology Utilization Reports and Notes, and Technology Surveys.

Details on the availability of these publications may be obtained from:

SCIENTIFIC AND TECHNICAL INFORMATION DIVISION

NATIONAL AERONAUTICS AND SPACE ADMINISTRATION

Washington, D.C. 20546